

Crustal underplating and effective elastic plate thickness of the Laxmi Ridge, northern Arabian Sea

Akhil Mishra^{1,2}, Chaubey A.K.^{1,2*}, Sreejith K.M.³ and Shravan Kumar¹

¹ CSIR-National Institute of Oceanography, Regional Centre, Lokhandwala Road,
Andheri (West), Mumbai-400053, India.

² Academy of Scientific and Innovative Research, CSIR-National Institute of Oceanography,
Goa, India.

³ Geosciences Division, ISRO-Space Applications Centre, Ahmedabad-380015, India.

*Corresponding Author's Email: chaubey@nio.org

Abstract

Laxmi Ridge, a prominent basement high feature with negative gravity anomaly in the northern Arabian Sea, is generally considered as stretched continental crust. However, recently it is proposed that the ridge could be an extinct spreading ridge. Ship-borne and satellite-altimetry derived bathymetry, gravity and geoid data over the Laxmi Ridge are analysed and modelled to determine effective elastic plate thickness (T_e) and crustal structure beneath the ridge. The estimation of T_e and compensation mechanism of the ridge are examined based on 3D coherence and admittance analysis considering surface and subsurface loads which involve computation of coherence and admittance between Mantle Bouguer Anomaly (MBA) and sediment corrected bathymetry. The best fit model reveals that T_e is about 3-4 km and amplitude of subsurface load at Moho is approximately equal to the surface load. Low value of T_e implies elastically weak lithospheric plate which can be attributed to either weakening of lithosphere by re-heating and underplating caused by the then nearby Réunion Hotspot or volcanic emplacement on the young oceanic crust. Further, all along the length of the Laxmi Ridge, the MBA is negative and its magnitude reaches up to 115 mGal, which indicates either presence of thickened crust or less dense mantle beneath the ridge. 2D crustal models suggest that underplating material is prevalent all along the Laxmi Ridge. High amplitude (>400 nT) magnetic anomaly over the southern part of the ridge reveals several lineations in WNW-ESE direction suggesting magma outpouring along weak zones. Geoid to topographic ratio over the ridge is negative (-1.98 m/km), possibly indicating shallow subsurface load (<20 km) with small wavelength (<200 km). Based on present study and available geophysical results, we infer that the Laxmi Ridge is a stretched continental sliver which is underplated, intruded by volcanics and isostatically compensated by Airy Model of Compensation.

Keywords: Laxmi Ridge, Effective elastic plate thickness, Coherence and Admittance, Mantle Bouguer Anomaly, Geoid to Topographic Ratio, Magnetic anomaly.

1. Introduction

Laxmi Ridge is a prominent basement high feature forming a submarine ridge and mostly buried under the Indus fan sediment in the northern Arabian Sea, northwestern Indian Ocean (Fig. 1). It runs in the NW-SE direction i.e., between 14.5°N and 19.3°N and then in the E-W direction from 19.3°N, 65.8°E onwards. The average water depth and maximum relief over the ridge are about 3.5 km and 1.2 km respectively. Its southernmost part is wider than the northernmost part. Bathymetric map reveals that its width varies from 40 km to 100 km, however, published crustal models suggest that the maximum width of the ridge reaches up to 200 km. The extent and trend of E-W part of the Laxmi Ridge are indiscernible in the bathymetric map while NW-SE part is well evident. In spite of being a basement high feature all along its extent and a bathymetrically positive feature at its southern end, the whole Laxmi Ridge is associated with a relative gravity low (Fig. 1). Both free air and isostatic gravity anomalies are relatively negative over it (Naini and Talwani, 1983) and the whole settlement of the Laxmi Ridge can be clearly seen in the free air anomaly (FAA) map. Magnetic anomaly across the Laxmi Ridge does not exhibit any regular pattern so couldn't be related to the seafloor spreading type magnetic anomaly.

Under the Laxmi Ridge, the Moho depth varies between 21 and 23 km (Minshull et al., 2008; Misra et al., 2015; Naini and Talwani, 1983), which implies that it is thicker than normal oceanic crust and thinner than the typical continental crust. Different opinions prevail for the nature of crust under the Laxmi Ridge. Some researchers opined that it is of continental origin (Ajay et al., 2010; Arora et al., 2012; Bhattacharya et al., 1994; Bhattacharya and Yatheesh, 2015; Krishna et al., 2006; Kalra et al., 2014; Naini and Talwani, 1983; Nair et al., 2015; Radhakrishna et al., 2002; Talwani and Reif, 1998; Todal and Edholm, 1998) while others argued that it is of oceanic origin (Misra et al., 2015 and references therein; Pandey et al., 1995; Singh, 1999).

No detailed study has been carried out for the determination of T_e and isostasy over the Laxmi Ridge. Though Bansal et al. (2005) and Ratheesh-Kumar et al. (2015) estimated T_e over the Laxmi Ridge based on regional study, however, the objectives of these two research papers were not the detailed isostatic investigation over the Laxmi Ridge. Also, some other noteworthy work exists in the literature dealing with the isostasy and T_e evaluation of the nearby areas (Ashalatha et al., 1991; Chand and Subrahmanyam, 2003; Chaubey et al., 2008; Dev et al., 2007; Radhakrishna and Searle, 2006; Tiwari et al., 2007). These research papers cover mostly isostasy mechanism of Laccadive Ridge, the western continental margin of India or Owen transform regions.

Ship-borne and satellite altimetry derived bathymetry, gravity and geoid data over the Laxmi Ridge are analysed and modelled to meet the major objectives of the present study which include (i) determination of the elastic plate thickness along the Laxmi Ridge based on coherence and admittance analysis (ii) investigation of isostatic compensation mechanism and subsurface loading along the ridge, (iii) establishment of crustal structure and nature of the ridge.

2. Regional Tectonics

Laxmi and Laccadive ridges divide the sedimentary basins of the Western Continental Margin of India (WCMI) and adjacent ocean basins into two basins (Fig. 1). The part of sedimentary basin west of Laxmi-Laccadive ridges is named as Western Basin and the part which is east of these ridges is known as Eastern Basin (Naini and Talwani, 1983). Laxmi Ridge possesses a significant history of early evolution of the WCMI and adjacent ocean basins. The published tectonic models suggest that the basins adjoining both sides of the Laxmi-Laccadive ridges have evolved due to break-up and rifting of India, Laxmi Ridge, Seychelles and Madagascar. Some researchers (Naini and Talwani, 1983; Norton and Sclater, 1979) have proposed two stages of rifting. In the first stage, India rifted from Madagascar during the mid-Cretaceous, and (ii) in the second stage, India-Laxmi Ridge rifted from Seychelles during the Early Tertiary. While others (Bhattacharya et al., 1994; Bhattacharya and Yatheesh, 2015; Chaubey et al., 2002; Minshull et al., 2008; Yatheesh et al., 2006) assert three stages of rifting which carved the WCMI and adjacent geological provinces, i.e. (i) rifting between India and Madagascar during the mid-Cretaceous, (ii) short span of rifting between Seychelles-Laxmi Ridge and India during the Late Cretaceous, and (iii) finally rifting between Laxmi Ridge-India and Seychelles during the early-Tertiary. The resulting structural features of the margin are tremendously modified by two geodynamic events (i) Réunion hotspot activity, and (ii) Indo-Eurasian continental collision.

Eastern Somali Basin and its conjugate Western Basin were formed by seafloor spreading across the then Carlsberg Ridge. Therefore, crust beneath both the basins is undoubtedly oceanic in nature and formed by propagating spreading ridge during the Paleogene (Chaubey et al., 1998, 2002; Dymant, 1998; Miles et al., 1998; Miles and Roest, 1993; Royer et al., 2002). The oldest magnetic anomaly identified in the Western Basin is C28ny, which is located just west of the Laxmi Ridge (Chaubey et al. 1998, 2002; Miles and Roest 1993). The evolutionary history of the region younger than C28ny is well documented but older is not yet established conclusively.

The nature of crust under the Eastern Basin, which comprises of Gop, Laxmi and Laccadive basins is not unequivocally established. Some researchers (Kolla and Coumes 1990; Krishna et al., 2006;

Naini and Talwani, 1983; Rao et al. 1992; Todal and Edholm 1998) believed that the Laxmi Basin is underlain by thin, stretched and intruded continental crust; while others (Bhattacharya et al., 1994; Bhattacharya and Yatheesh, 2015; Biswas and Singh, 1988; Eagles and Wibisono, 2013; Ramana et al., 2015; Talwani and Reif, 1998) favor its oceanic origin. Bhattacharya et al. (1994) recognised correlatable seafloor spreading type symmetric magnetic anomaly in the Laxmi Basin and suggested Panikkar Ridge as an extinct spreading centre, whereas, Krishna et al. (2006) interpreted these magnetic anomalies due to volcanic intrusive within the stretched continental crust. Recently, Pandey and Pandey (2015) categorised the crust in the Laxmi Basin into two zones; the first one is stretched zone having fault-bounded horst and graben structure and the second one is highly intruded transitional crust. During the International Ocean Discovery Program (IODP) Expedition 355, two sites (U1456 and U1457) were drilled in the eastern Arabian Sea. Site U1456, located in the Laxmi Basin, penetrated 1109.4 m below seafloor and recovered oldest sediment dated 17.7 Myr. Whereas site U1457, located on northeastern flank of the Laxmi Ridge, penetrated 1108.6 m below seafloor and could recover massive basalt as well as associated volcano-clastic sediment. Preliminary geochemical analysis showed that the recovered basalts were characteristic of low-K and with high-Mg subalkaline tholeiitic basalt that do not represent typical mid-oceanic ridge basalt (Pandey et al., 2015). Therefore, till date, the nature of crystalline crust of the Laxmi Basin is unclear.

Further, though the crustal nature of the Gop Basin is well established as oceanic (Collier et al., 2008; Malod et al., 1997; Minshull et al., 2008; Ramana et al., 2015; Yatheesh et al. 2009) different opinions exist regarding the identification of older magnetic lineation and location of extinct spreading centre (Bhattacharya and Yatheesh, 2015). In summary, the Laxmi Ridge is sandwiched between pure oceanic crust of the Western Basin and debatable crust of the Laxmi Basin.

3. Data

Ship-borne bathymetry, gravity and magnetic data used in the present study were collected during different cruises of ORV Sagar Kanya (SK64, SK79, and SK162) and RV Sindhu Sankalp (SSK96) during 1991-2016. The bathymetry, gravity data and magnetic data in cruises SK64, SK79 and SK162 were acquired using deep sea echosounder (M/S. Honeywell Elac), marine gravimeter KSS30 and Proton Precession Magnetometer (PPM) G801/3, respectively with satellite based navigation system (GPS, Model MX 4400). Magnetic data were acquired using cesium vapor magnetometer G882 during the cruise SSK96 with satellite based navigation (Hemisphere R220 GPS Receiver). The surveyed tracks are shown in Figure 1. From all the profiles, spikes and other erroneous data were removed. Total magnetic field intensity data have been reduced to residual magnetic anomalies

by subtracting the International Geomagnetic Reference Field (IGRF) for the years 1992 and 2016 for magnetic acquired during cruises SK79 and SSK096, respectively. The free air gravity anomalies were obtained by applying normal and Eötvös corrections to the measured gravity data. Both the ship-borne bathymetry and gravity data were first smoothed by filtering using 5 km Gaussian Filter and then resampled at 0.4 km interval for crustal structure modelling across the Laxmi Ridge.

In addition to ship-borne data, satellite data have also been used in the present study. For bathymetry data, 'bedrock' version of ETOPO1, one arc-minute global relief model which were generated from diverse global and regional digital data sets (Amante and Eakins, 2009), have been utilised. Free-air anomaly data are obtained from global marine gravity data (grav.img.24.1) of Sandwell et. al. (2014) which are derived by combining altimetry measurements from satellites CryoSat-2 and Jason-1 with existing data (Fig. 1).

The sediment thickness model, utilised in this work, is taken from Divins (2003). The geoid grid for the study area was extracted from geoid data generated for the northern Indian Ocean by Sreejith et al. (2013). Average P-wave velocity for each crustal layers have been calculated using refraction data of the Western and Eastern basins (Naini and Talwani, 1983) covering the Laxmi Ridge (Fig. 1). These average velocities have been converted into density using Brocher (2005) formula for forward gravity modelling and are shown in Table 1.

4. Theory and Method

4.1 Admittance and Coherence analysis

The analysis of gravity and bathymetry data in spectral domain offers two very important parameters viz. admittance and coherence which can be used to determine the mode of isostatic compensation of lithosphere. Admittance relates gravity and bathymetry in wave number domain by a transfer function, and coherence provides a measure of the fraction of gravity that can be predicted from bathymetry (McKenzie and Bowin, 1976; Watts, 1978; Watts, 2001).

The theoretical admittance between MBA and sediment corrected bathymetry for the surface load (i.e. top load, Z_T) and subsurface load (i.e. bottom load, Z_B) can be computed using following formula given by Neumann and Forsyth (1993):

$$Z_T(k) = -2\pi G e^{-2\pi k d} \Delta\rho_m \frac{\theta}{\xi}, \dots\dots\dots (1)$$

$$Z_B(k) = -2\pi G e^{-2\pi k d} \Delta\rho_m \theta, \dots\dots\dots (2)$$

where
$$\theta = 1 + \frac{D(2\pi k)^4}{\Delta\rho_m g}, \dots\dots\dots (3)$$

$$\xi = 1 + \frac{D(2\pi k)^4}{\Delta\rho g}, \dots\dots\dots (4)$$

$$D = \frac{ET_e^3}{12(1-\sigma^2)}, \dots\dots\dots (5)$$

$$\Delta\rho = \rho_m - \rho_c \text{ and } \Delta\rho_m = \rho_m - \rho_w$$

Where, D is flexural rigidity. Other notations and their values are presented in Table 2.

Assuming top and bottom loads are independent, the expression for combined theoretical admittance (Z) can be given as the weighted average of both loading and resulting equation (Forsyth, 1985; Neumann and Forsyth, 1993) can be written as:

$$Z(k) = -2\pi G e^{-2\pi k d} \Delta\rho_m \theta \frac{(F^2 + \xi)}{(F^2 + \xi^2)}. \dots\dots\dots (6)$$

Where F is subsurface to surface load ratio. The observed admittance is computed from the bathymetry and gravity data using following formula:

$$Z(k) = \frac{\langle G(k)B^*(k) \rangle}{\langle B(k)B^*(k) \rangle}. \dots\dots\dots (7)$$

B(k) is the Fourier transform of sediment corrected bathymetry and G(k) is the Fourier transform of MBA. The asterisk (*) denotes the complex conjugate and ⟨ ⟩ denotes annular averaging in wave number band.

The classical way of determining T_e is to compare the observed admittance with the theoretical one. The Theoretical admittance is calculated for the surface and subsurface load by changing independent parameters T_e and F (subsurface to surface load ratio) which leads to different models of isostasy. Different models with different T_e give rise non-unique interpretation because a strong plate with the subsurface load may produce the same response as a weak plate with the surface load (Forsyth, 1985; Luis and Neves, 2006; Sreejith and Krishna, 2013). To overcome the obscurity which arises due to the presence of both subsurface and surface load, an alternative method is developed which utilises the coherence function instead of admittance between MBA and sediment corrected bathymetry (Forsyth, 1985; Neumann and Forsyth, 1993; Luis and Neves, 2006; Sreejith and Krishna, 2013). This approach can be used to constrain the value of T_e as well as to discriminate different isostatic models.

The theoretical coherence between MBA and sediment corrected bathymetry can be computed from:

$$\gamma^2(k) = \frac{(1+(F/\xi)^2\phi)^2}{(1+(F/\xi)^2)(1+F^2\phi^2)}, \dots\dots\dots (8)$$

where, $\phi = 1 + \frac{D(2\pi k)^4}{(\rho_c - \rho_w)g} \dots\dots\dots (9)$

The observed coherence is computed by the following relation:

$$\gamma^2(k) = \frac{C(k)C^*(k)}{E_g(k)E_b(k)} \dots\dots\dots (10)$$

Where C(k) is the cross-spectrum of bathymetry and gravity; The asterisk (*) denotes the complex conjugate; E_g(k) and E_b(k) are the power spectrums of gravity and bathymetry, respectively.

4.2 Forward Gravity Model

2D forward gravity modelling has been carried out using GM-SYS module of Oasis Montaj software. The computational scheme is based on the method of Talwani et. al. (1959) and makes use of algorithms illustrated in Won and Bevis (1987). The GM-SYS module calculates the gravitational attraction of two-dimensional bodies of arbitrary shape approximated by an n-sided polygon with constant density. To eliminate the edge effect, all GM-SYS models are extended to ± 30000 km (infinity) in the X direction. In forward gravity modelling, a hypothetical geological model is created and its gravity response is calculated to compare with observed gravity value. If there is a good match between observed and calculated gravity then the hypothetical model is the final crustal model, if not, then in an interactive way, the hypothetical model is kept on modifying till the best match is obtained.

As a first step, an initial crustal model is prepared along a selected transect by integrating bathymetry, seismic reflection and refraction data available along the transect, if not, from the adjacent region. Main crustal layers are identified based on velocities determined by seismic reflection and refraction data. Average velocity of each layer is calculated and density of the layer is computed using velocity-density formula provided by Brocher (2005). Forward gravity modelling was performed by continuously applying small adjustments to the geometries of crustal layers in order to obtain a crustal model which satisfies both the geometrical constraints and an acceptable fit between observed and calculated gravity anomalies.

5. Analysis and Interpretation

5.1 Calculation of MBA and sediment corrected bathymetry

MBA data of the study area are generated by subtracting gravity effect of seafloor relief, sediments and crust-mantle interface from Free-air Gravity Anomaly (FAA) assuming an average crustal thickness of 6 km. The MBA map of the study area is shown in Figure 2. To get sediment corrected bathymetry, sediment thickness is multiplied by a correction factor 0.48 (Crough, 1983) to remove its isostatic effect and then subtracted from the bathymetry derived through satellite altimetry. Computation of gravity anomaly from bathymetry and density contrast is carried out using an algorithm developed by Parker (1972).

5.2 Mantle Bouguer Anomaly and coherence analysis

The coherence between MBA and sediment corrected bathymetry is computed using Eq. 10 for the region encompassing the Laxmi Ridge (Fig. 2). The computed coherence as a function of wavelength is shown in Figure 3a. For the long wavelength range (>400 km), the coherence is almost unity which is an indication of locally compensated topography with Airy-type isostasy, suggesting that bathymetry is not supported by flexural strength of the lithosphere. The coherence for the wavelength less than 50 km displays noise influenced values, therefore these values are not considered for analysis. The wavelength of the transition zone from low coherence to high coherence provides an indication of flexural rigidity of the lithosphere and in this zone (50 km to 250 km), observed coherence values rise sharply from 0.15 to 0.80.

The theoretical coherence between MBA and corrected bathymetry is computed as a function of wavelength from Eq. 8, for a range of loading ratio (F) and T_e values (Fig. 3a). Theoretical coherence, for $T_e=2, 3, 5, 7$ km and for a fixed value of $F=0.8$, are plotted (Fig. 3a, blue coloured curve) on a semi-logarithmic graph together with observed coherence (Fig. 3a, stars with error-bars in red colour) for comparison. The values of observed coherence are falling between the theoretical coherence curves computed with $T_e=3$ km and 5 km. Inferred T_e range (3-5 km, Fig. 3a) indicate same tectonic setting so there could not be much variation in compensation mechanism all along the ridge. The narrow width of the transition zone (50-250 km) is suggestive of similar T_e trend along the Laxmi Ridge.

For constraining the values of T_e and load ratio F , Root Mean Square (RMS) error between observed and theoretical coherence is examined. The value of T_e and F are systematically varied from 0.0001 km to 20 km and from 0 to 5 respectively to compute the RMS error. For each combination of T_e and

F, the rms error between theoretical and observed coherence is calculated and plotted against T_e and F (Figure 3b). The result shows that the RMS error is minimum for $T_e=3.3$ km and $F=0.8$ which is shown by a star in Figure 3b. This implies that the amplitude of subsurface load at Moho is almost equal (80 %) to that of the surface load. The coherence curve for the best match ($T_e=3.3$ km and $F=0.8$.) is shown with green colour in Figure 3a. Therefore, it is interpreted that the elastic plate thickness of the Laxmi Ridge is low and the plate is weak.

5.3 MBA and admittance analysis

To put another constraint on the elastic plate thickness, admittance analysis between MBA and sediment corrected bathymetry has also been carried out over the same region. The admittance between MBA and corrected bathymetry is computed using Eq. 7 and displayed in Figure 3c. The observed admittance values, for the wavelength shorter than 50 km, consist of noise influenced values whereas, for long wavelength (>300 km) admittance values lie between 0.08 and 0.09 mGal/km (Fig. 3c).

It is well known that coherence is more sensitive to F value. Therefore, the value of 0.8 determined by coherence analysis is adopted while computing theoretical admittance using Eq. 6.

The theoretical admittance for combined load (surface and sub-surface) is calculated for $T_e=2, 3, 4$ km and presented along with the observed admittance in Figure 3c. The observed admittance values (for wavelength range 50-300 km) are falling in between theoretical curves of $T_e=1$ km and $T_e=3$ km (Fig. 3c). It may be mentioned here that the elastic plate thickness obtained from coherence study is 3.3 km. Therefore, elastic plate thickness determined by two independent methods (the coherence and admittance) is in good concurrence and suggests that the Laxmi Ridge is supported by elastically weak lithospheric plate.

5.4 Geoid anomaly and geoid to topography ratio

It is well known that the longer wavelength (>4000 km) geoid and topographic anomalies are due to density anomalies in the lower mantle (Bowin, 1983) and cooling of the lithosphere (Haxby and Turcotte, 1978) while shorter wavelength (<330 km) contain signal from lithosphere flexure and variation in crustal thickness. However, geoid is linearly related to the topography between wavelengths 330 and 4000 km (Sandwell & Renkin 1988), therefore, the Geoid to Topography Ratio (GTR) analysis of these waveband can be used to understand isostatic compensation mechanism of oceanic features (Haxby and Turcotte, 1978; Sandwell and Mckenzie, 1989).

Gridded geoid height and sediment corrected bathymetry data sets of entire western Indian Ocean were filtered to pass 330-4000 km wavelength to generate residual geoid and topography (Figures 4 a and b). In general, the Laxmi Ridge is associated with negative residual geoid values of -0.2 m to -4.5 m. We also note strong gradient in geoid heights along the axis of the ridge from south (low geoid) to north (high). In contrast, the residual topography is high (0-500 m) towards south and low (-200 to 50 m) towards north.

For GTR analysis, a polygon was selected to sample the Laxmi Ridge without including adjacent geological features such as seamounts, continental margin etc so that results are not influenced by any artifacts. GTR is computed by taking the slope of the best-fitting least square regression line through the scatter plot of residual topography and geoid (Fig. 4c). The calculated GTR over the Laxmi Ridge is negative (-1.98 m/km, Fig. 4c). In general, the GTR values are grouped into three ranges; (i) 0-2 m/km indicating shallow compensation (ii) 2-6 m/km corresponds to thermal isostasy and (iii) >6 m/km indicating sub-lithospheric compensation supported by mantle convection. Interestingly, negative GTR values are not given much attention in the literature, though reported over several prominent features (Table-3).

Negative GTR observed over several plateaus and ridges were (eg. Rockall Plateau) initially suspected due to an artefact (Sandwell and Mackenzie, 1989) or caused by poor quality and low resolution data (Marks and Sandwell, 1991). Later on, some other researchers (Heller and Marquart, 2002; Rao et al., 2016) have also found negative GTR (Table 3) even using high resolution data sets. Similar to the case of Laxmi Ridge, several plateaus/ridges of the world ocean (Table 3) possess negative GTR which are generally thought to be related with shallow structural and density heterogeneities. Considering the negative gravity anomaly, low T_e of 3-4 km and a loading ratio of 0.8, we interpret that the negative GTR of the Laxmi Ridge could be caused by shallow subsurface load (<20 km) with small wavelength (<200 km) as in the case of Voring Plateau (Heller and Marquart, 2002).

5.5 Magnetic anomaly

The magnetic anomaly along several N-S tracks is plotted on a histogram equalized Vertical Gravity Gradient (VGG) map over the southern part of the Laxmi Ridge (Fig. 5). The high amplitude (>400 nT) magnetic anomaly reveals several lineations (LR-1 to LR-4) in WNW-ESE direction and also correspond to lineations in VGG map. Both the magnetic and VGG lineation are of limited extent and lie within boundary of the Laxmi Ridge. These observations suggest that the local magnetic

lineation are due to magma outpouring along weak zones. One of the prominent magnetic lineations (LR-1) with high amplitude anomaly indicates that southern part of the Laxmi Ridge might have undergone rifting episode in which southernmost block of the ridge had tried to split from remaining part of the ridge. It may be noted that boundary of the Laxmi Ridge is also disrupted near the lineation LR-1. Magnetic lineation with high amplitude magnetic anomaly suggests that the Laxmi Ridge is associated with several weak zones and is intruded by volcanics.

5.6 2D Gravity Modelling

Ship-borne Free-air gravity anomaly profiles along transects SK64-02 (which traversed across the E-W part of the Laxmi Ridge) and transects SK162-09 and SK162-13 (which traversed across the NW-SE part of the Laxmi Ridge) have been selected for crustal structure modelling (Figs. 6a-6c). Modelling along these transects have been carried out under the constraints from published (i) crustal velocity model derived from refraction data (Naini and Talwani, 1983), (ii) nearby seismic reflection data (RE01, RE02 and RE11) and (iii) crustal model derived from OBS data (Minshull et al., 2008). The gravity and bathymetry data along these profiles are filtered using a Gaussian filter of width 5 km and then resampled at an interval of 0.4 km. The density for sediment has been taken as 2.2 g/cm³, oceanic layer-2 as 2.62 g/cm³ and oceanic layer-3 as 2.88 g/cm³. Broadly, 4 crustal layers have been considered below the Laxmi Ridge and densities for these layers have been taken as 2.46, 2.60, 2.78 and 3.03 g/cm³ (Table-1). In all crustal models (Figs. 6a, b, c), the layer of density 2.46 gm/cm³ correspond to flood basalt. The flood basalt layer, lie below the sedimentary layer, carpeted the Laxmi Ridge and is an expression of surface volcanism. The best fit models reveal that the crustal thickness (excluding sediments) of the Laxmi Ridge varies from 15 to 18 km. The Laxmi Ridge and the Laxmi Basin, both are underlain by a high density underplated layer and its thickness varies from ~4 to 10 km along the modelled profiles. The refraction stations L04, L05, L07 over the Laxmi Ridge and refraction stations L09, L11, L06, L10 (Naini and Talwani, 1983) in the Laxmi Basin, have reported high density (high velocity ~7.2 km/s) layer of thickness ~ 5 to 10 km. In addition, based on the OBS data, Minshull et al. (2008) have also found high density underplated layer with maximum thickness ~8 km below the E-W part of the Laxmi Ridge. Flood basalt volcanism, intrusions (like LR-1 to LR-4 in Fig. 5 and intrusion in Fig. 6c) and rifting signature along LR-1 (Fig. 5) further support the existence of underplated layer. The underplated layer contributed significantly to negative gravity anomaly observed over the Laxmi Ridge.

We have also modelled the crustal structure along profile SK162-09 with lesser thickness of underplated layer for an uncertainty analysis (Fig. 7). The effect of thinning of underplated layer is

calculated by keeping the Moho depth and sediment thickness fixed. When the thickness of underplated layer is decreased by 3 km as compared to the best fit model, all other crustal layers are proportionally thickened. It gives a large mismatch between observed and calculated gravity anomalies (Fig. 7) and the RMS error rises to 12.38 mGal as compared to 0.59 mGal for best fit model (Fig. 6b). Thus, it is unlikely to generate best fit crustal model with lesser thickness of underplated layer.

6. Results and Discussion

The effective elastic plate thickness of the Laxmi Ridge as determined from two independent methods (coherence and admittance) is about 3 to 4 km with subsurface to surface load ratio of 0.8. Low T_e value obtained in the present study is in good agreement with that of Ratheesh-Kumar et al. (2015) where they found $T_e=2-4$ km based on flexural modelling in the spatial domain (convolution method). However, using Bouguer admittance, Bansal et al. (2005) suggested slightly higher value of T_e i.e. 6-8 km for the Laxmi Ridge. The slight discrepancy in the T_e values may be due to the selection of different window size (block 9 of Figure 1 in Bansal et al., 2005) and model parameters adopted for the computation.

The low value of T_e observed in this study implies that crustal nature of the Laxmi Ridge could be either oceanic or thinned/fractured continental crust. For the Laxmi Ridge to be oceanic or extinct spreading centre, magnetic signature should support linear magnetic stripes but till date available magnetic data could not be correlated to any seafloor spreading type magnetic signature. Further P-wave velocity structures over the Laxmi Ridge and well known oceanic crust, west of the ridge are totally different. Also, the crustal models (Figs. 6a-6c) along several transects across the ridge do not support the oceanic nature of the crust. Therefore, we negate the possibilities of the Laxmi Ridge being oceanic in nature.

The low value of T_e implies that the Laxmi Ridge is compensated locally (Airy Type) and the lithosphere is elastically weak beneath the ridge. The present study also reveals that amplitude of subsurface load is almost equal to that of surface load ($F=0.8$) which implies that the subsurface processes played a significant role for weakening the underlying lithosphere beneath the ridge. From the evolutionary history of the western continental margin of India and adjacent ocean basins, it is evident that the Laxmi Ridge had undergone two major rifting episodes at both of its eastern and western ends. In the first stage, rifting occurred when Seychelles-Laxmi Ridge were together and got separated from India during the Late Cretaceous. In the second rifting stage, conjoined Laxmi Ridge-

India separated from Seychelles during the early-Tertiary. Since rifting is always associated with stretching, fracturing and dispersal events, therefore these processes must have contributed substantially in reducing the lithospheric strength.

Therefore, keeping in mind tectonic history of the WCMI, two major factors of lithospheric deformation can be taken into account which caused low value of T_e : (i) deformation as a result of various rifting processes (stretching, crustal necking, crustal thinning, fracturing, volcanic loading etc.) between India, Madagascar, Seychelles Laxmi Ridge during mid-Cretaceous to early Tertiary; and (ii) deformation caused by Réunion hotspot from 67 Ma to 60 Ma. Out of these two, which factor dominated for lowering the value of T_e needs to be established through a rigorous approach to understand their relative importance. The study carried out by Watts (1988) and Watts and Fairhead (1997) revealed that the continental lithosphere could not acquired any significant long term strength following a rifting event. Further, Watts and Fairhead (1997) suggested that either the strength of stretched crust recovers on much longer (>200 ma) time-scales than the oceanic lithosphere or, that during rifting the strong uppermost part of the crust is somehow decoupled from any support that it might otherwise have received from the cooling and strengthening of the underlying mantle.

From the present value of subsurface to surface load ratio of $F=0.8$ determined over the Laxmi Ridge when compared with the F values derived over 90° East Ridge (NER) in other studies (e.g. Grevemeyer et al., 2001, Sreejith and Krishna 2013), it can be concluded that the extent of underplating material under the Laxmi Ridge must be comparatively large. In the case of NER, F value determined from coherence and admittance analysis (Grevemeyer et al., 2001, Sreejith and Krishna 2013), is slightly greater than 0.5 and from seismic survey, the volume ratio of subsurface to surface load was constrained to be about 0.7 (Grevemeyer et al., 2001). The maximum thickness of underplated material in the NER was interpreted around 5 km. The F value obtained in the present study is higher than that of NER and thickness of underplating beneath the Laxmi Ridge as seen in the crustal model from forward gravity model of present study and also that of Minshull et al. (2008) is about 8 km.

7. Conclusions

Analyses of coherence and admittance between MBA and sediment corrected bathymetry, geoid, GTR, forward gravity models and magnetic anomaly carried out in the present study, provide new understanding on elastic plate thickness, isostatic compensation, subsurface loading and crustal nature of the Laxmi Ridge. Major findings of the study are summarized as follows:

- i. The effective elastic plate thickness of the Laxmi Ridge as determined from coherence between MBA and sediment corrected bathymetry, is about 3 to 4 km with subsurface to surface load ratio of 0.8.
- ii. The Laxmi Ridge is underplated all along its length and thickness of maximum underplating is about 8 km.
- iii. Low value of T_e implies that the Laxmi Ridge is compensated locally (Airy Type) and the lithosphere is elastically weak beneath the ridge.
- iv. Low value of T_e is caused by various rifting processes (stretching, crustal necking, crustal thinning, fracturing, volcanic loading etc.) between India, Madagascar, Seychelles and Laxmi Ridge during mid-Cretaceous to early Tertiary and reheating of the lithosphere by Réunion hotspot from 67 Ma to 60 Ma.
- v. The calculated GTR over the Laxmi Ridge is negative (-1.98 m/km) and indicates shallow subsurface loading.
- vi. Magnetic lineation with high amplitude magnetic anomaly suggests that the Laxmi Ridge is associated with several weak zones and is intruded by volcanics. One of the prominent magnetic lineation with high amplitude anomaly near southern part of the Laxmi Ridge indicates that this portion might have undergone rifting episode in which southernmost block of the ridge had tried to split from remaining part of the ridge.

Acknowledgments

The authors are thankful to Prof. Sunil Kumar Singh, Director, CSIR-National Institute of Oceanography, Goa and Dr. A.S. Rajawat, ISRO-SAC, Ahmedabad for support and encouragement in this work. This work was carried out jointly by CSIR-NIO and ISRO-SAC as a part of the MOP III–Marine Lithospheric Studies program. We are also grateful for the critical review and constructive comments by two anonymous reviewers, which helped to improve the manuscript. Figures (except Figs. 6 and 7) were prepared using GMT software of Wessel and Smith (1998). Akhil Mishra acknowledges the Council of Scientific and Industrial Research, for financial support as JRF & SRF. This is NIO contribution no. ????.

References

- Ajay, K.K., Chaubey, A.K., Krishna, K.S., Rao, D.G., Sar, D., 2010. Seaward dipping reflectors along the SW continental margin of India: Evidence for volcanic passive margin. *Journal of earth system science* 119, 803-813.
- Amante, C., Eakins, B.W., 2009. ETOPO1 1 Arc-Minute Global Relief Model: Procedures, Data Sources and Analysis. NOAA Technical Memorandum NESDIS NGDC-24. National Geophysical Data Center, NOAA. doi:10.7289/V5C8276M.
- Arora, K., Tiwari, V.M., Singh, B., Mishra, D.C., Grevemeyer, I., 2012. Three dimensional lithospheric structure of the western continental margin of India constrained from gravity modelling: implication for tectonic evolution. *Geophysical Journal International* 190, 131-150.
- Ashalatha, B., Subrahmanyam, C., Singh, R.N., 1991. Origin and compensation of Chagos-Laccadive ridge, Indian ocean, from admittance analysis of gravity and bathymetry data. *Earth and Planetary Science Letters* 105, 47-54.
- Bansal, A.R., Fairhead, J.D., Green, C.M., Fletcher, K.M.U., 2005. Revised gravity for offshore India and the isostatic compensation of submarine features. *Tectonophysics* 404, 1-22.
- Bhattacharya, G.C., Chaubey, A.K., Murty, G.P.S., Srinivas, K., Sarma, K.V.L.N.S., Subrahmanyam, V., Krishna, K.S., 1994. Evidence for seafloor spreading in the Laxmi Basin, northeastern Arabian Sea. *Earth and Planetary Science Letters* 125, 211-220.
- Bhattacharya, G.C., Yatheesh, V., 2015. Plate-Tectonic Evolution of the Deep Ocean Basins Adjoining the Western Continental Margin of India—A Proposed Model for the Early Opening Scenario, in: Mukherjee, S. (Ed.), *Petroleum Geosciences: Indian Contexts*. Springer International Publishing, Cham, pp. 1-61.
- Biswas S.K., Singh N.K., 1988. Western continental margin of India and hydrocarbon potential of deep-sea basins. In: 7th Offshore Southeast Asia conference, Singapore OTSC 88119, pp. 170–181.
- Bowin, C., 1983. Depth of principal mass anomalies contributing to the earth's geoidal undulations and gravity anomalies. *Marine Geodesy* 7, 61-100.
- Brocher, T.M., 2005. Empirical Relations between Elastic Wavespeeds and Density in the Earth's Crust. *Bulletin of the Seismological Society of America* 95, 2081-2092.
- Chand, S., Subrahmanyam, C., 2003. Rifting between India and Madagascar – mechanism and isostasy. *Earth and Planetary Science Letters* 210, 317-332.
- Chaubey, A.K., Bhattacharya, G.C., Murty, G.P.S., Srinivas, K., Ramprasad, T., Rao, D.G., 1998. Early Tertiary seafloor spreading magnetic anomalies and paleo-propagators in the northern Arabian Sea. *Earth and Planetary Science Letters* 154, 41-52.
- Chaubey, A.K., Dymant, J., Bhattacharya, G.C., Royer, J.-Y., Srinivas, K., Yatheesh, V., 2002. Paleogene magnetic isochrons and palaeo-propagators in the Arabian and Eastern Somali basins, NW Indian Ocean. *Geological Society, London, Special Publications* 195, 71-85.

- Chaubey, A.K., Srinivas, K., Ashalatha, B., Rao, D.G., 2008. Isostatic response of the Laccadive Ridge from admittance analysis of gravity and bathymetry data. *Journal of Geodynamics* 46, 10-20.
- Collier, J.S., Sansom, V., Ishizuka, O., Taylor, R.N., Minshull, T.A., Whitmarsh, R.B., 2008. Age of Seychelles–India break-up. *Earth and Planetary Science Letters* 272, 264-277.
- Crough, S.T., 1983. The correction for sediment loading on the seafloor. *Journal of Geophysical Research: Solid Earth* 88, 6449-6454.
- Dev, S.V., Radhakrishna, M., Subrahmanyam, C., 2007. Estimates of Effective Elastic Thickness along the Southwest Continental Margin of India Using Coherence Analysis of Gravity and Bathymetry Data - Geodynamic Implications. *Geological Society of India; Volume 70 , Issue 3 , September 2007.*
- Divins, D.L., 2003. Total Sediment Thickness of the World's Oceans & Marginal Seas, NOAA National Geophysical Data Center, Boulder, CO.
- Dyment, J., 1998. Evolution of the Carlsberg Ridge between 60 and 45 Ma: Ridge propagation, spreading asymmetry, and the Deccan-Reunion hotspot. *Journal of Geophysical Research: Solid Earth* 103, 24067-24084.
- Eagles, G., Wibisono, A.D., 2013. Ridge push, mantle plumes and the speed of the Indian plate. *Geophysical Journal International* 194, 670-677.
- Forsyth, D.W., 1985. Subsurface loading and estimates of the flexural rigidity of continental lithosphere. *Journal of Geophysical Research: Solid Earth* 90, 12623-12632.
- Grevenmeyer, I., Flueh, E.R., Reichert, C., Bialas, J., Kläschen, D., Kopp, C., 2001. Crustal architecture and deep structure of the Ninetyeast Ridge hotspot trail from active-source ocean bottom seismology. *Geophysical Journal International* 144, 414-431.
- Haxby, W.F., Turcotte, D.L., 1978. On isostatic geoid anomalies. *Journal of Geophysical Research: Solid Earth* 83, 5473-5478.
- Heller, D.A., Marquart, G., 2002. An admittance study of the Reykjanes Ridge and elevated plateaux between the Charlie-Gibbs and Senja fracture zones. *Geophysical Journal International* 148, 65-76.
- Kalra, R., Srinivasa Rao, G., Fainstein, R., Radhakrishna, M., Bastia, R., Chandrashekar, S., 2014. Crustal architecture and tectono-magmatic history of the western offshore of India: Implications on deepwater sub-basalt hydrocarbon exploration. *Journal of Petroleum Science and Engineering* 122, 149-158.
- Kolla, V., Coumes, F., 1990. Extension of structural and tectonic trends from the Indian subcontinent into the Eastern Arabian Sea. *Marine and petroleum Geology* 7, 188-196.
- Krishna, K.S., Rao, D.G., Sar, D., 2006. Nature of the crust in the Laxmi Basin (14°–20°N), western continental margin of India. *Tectonics* 25. doi:10.1029/2004tc001747.
- Luis, J.F., Neves, M.C., 2006. The isostatic compensation of the Azores Plateau: A 3D admittance and coherence analysis. *Journal of Volcanology and Geothermal Research* 156, 10-22.

- Malod, J.A., Droz, L., Kemal, B.M., Patriat, P., 1997. Early spreading and continental to oceanic basement transition beneath the Indus deep-sea fan: northeastern Arabian Sea. *Marine geology* 141, 221-235.
- Marks, K.M., Sandwell, D.T., 1991. Analysis of geoid height versus topography for oceanic plateaus and swells using nonbiased linear regression. *Journal of Geophysical Research: Solid Earth* 96, 8045-8055.
- Marquart, G., 1991. Interpretations of geoid anomalies around the Iceland hotspot. *Geophysical Journal International* 106, 149-160.
- McKenzie, D., Bowin, C., 1976. The relationship between bathymetry and gravity in the Atlantic Ocean. *Journal of Geophysical Research* 81, 1903-1915.
- Miles, P.R., Munsch, M., Ségoufin, J., 1998. Structure and early evolution of the Arabian Sea and East Somali Basin. *Geophysical Journal International* 134, 876-888.
- Miles, P.R., Roest, W.R., 1993. Earliest sea-floor spreading magnetic anomalies in the north Arabian Sea and the ocean-continent transition. *Geophysical Journal International* 115, 1025-1031.
- Minshull, T.A., Lane, C.I., Collier, J.S., Whitmarsh, R.B., 2008. The relationship between rifting and magmatism in the northeastern Arabian Sea. *Nature Geoscience* 1, 463-467.
- Misra, A.A., Sinha, N., Mukherjee, S., 2015. Repeat ridge jumps and microcontinent separation: insights from NE Arabian Sea. *Marine and petroleum Geology* 59, 406-428.
- Naini, B.R., Talwani, M., 1983. Structural framework and the evolutionary history of the continental margin of western India. Watkins, J.S., Drake, C.L. (Eds.), *Studies in Continental Margin Geology* Am. Assoc. Pet. Geol. Mem. 34, 167-191.
- Nair, N., Anand, S., Rajaram, M., Rao, P.R., 2015. A relook into the crustal architecture of Laxmi Ridge, northeastern Arabian Sea from geopotential data. *Journal of earth system science* 124, 613-630.
- Neumann, G.A., Forsyth, D.W., 1993. The paradox of the axial profile: Isostatic compensation along the axis of the Mid-Atlantic Ridge? *Journal of Geophysical Research: Solid Earth* 98, 17891-17910.
- Norton, I.O., Sclater, J.G., 1979. A model for the evolution of the Indian Ocean and the breakup of Gondwanaland. *Journal of Geophysical Research: Solid Earth* 84, 6803-6830.
- Pandey, A., Pandey, D.K., 2015. Mechanism of crustal extension in the Laxmi Basin, Arabian Sea. *Geodesy and Geodynamics* 6, 409-422.
- Pandey, D.K., Clift, P.D., Kulhanek, D.K., Andò, S., Bendle, J.A.P., Bratenkov, S., Griffith, E.M., Gurusurthy, G.P., Hahn, A., Iwai, M., Khim, B.-K., K., A., K., A.G., L., H.M., L., H., Lyle, M.W., , Mishra, R., Radhakrishna, T., Routledge, C.M., Saraswat, R., Saxena, R., Scardia, G., Sharma, G.K., Singh, A.D., Steinke, S., Suzuki, K., Tauxe, L., Tiwari, M., Xu, Z., and Yu, Z., 2015. Expedition 355 Preliminary Report: Arabian Sea Monsoon. International Ocean Discovery Program. <http://dx.doi.org/10.14379/iodp.pr.355.2015>.

- Pandey, O.P., Agrawal, P.K., Negi, J.G., 1995. Lithospheric structure beneath Laxmi Ridge and late Cretaceous geodynamic events. *Geo-Marine Letters* 15, 85-91.
- Parker, R.L., 1972. The Rapid Calculation of Potential Anomalies. *Geophysical Journal International* 31, 447-455.
- Radhakrishna, M., Searle, R.C., 2006. Isostatic response of the Alula-Fartak and Owen transforms in the Eastern Gulf of Aden and the adjoining Arabian Sea. *Geophysical Journal International* 165, 62-72.
- RadhaKrishna, M., Verma, R.K., Purushotham, A.K., 2002. Lithospheric structure below the eastern Arabian Sea and adjoining West Coast of India based on integrated analysis of gravity and seismic data. *Marine Geophysical Researches* 23, 25-42.
- Ramana, M.V., Desa, M.A., Ramprasad, T., 2015. Re-examination of geophysical data off Northwest India: Implications to the Late Cretaceous plate tectonics between India and Africa. *Marine geology* 365, 36-51.
- Rao, D.G., M.V., R., G.C., B., Subba Raju, L.V., Kamesh Raju, K.A., Ramprasad, T., 1992. Marine geophysical studies along a transect across the continental margin off Bombay coast, west of India. In: Desai, B.N. (Ed.), *Oceanography of the Indian Ocean*. IBH Publications, pp. 493-501.
- Rao, G.S., Radhakrishna, M., Sreejith, K.M., Krishna, K.S., Bull, J.M., 2016. Lithosphere Structure and upper mantle characteristics below the Bay of Bengal. *Geophysical Journal International*.
- Ratheesh-Kumar, R.T., Ishwar-Kumar, C., Windley, B.F., Razakamanana, T., Nair, R.R., Sajeev, K., 2015. India–Madagascar paleo-fit based on flexural isostasy of their rifted margins. *Gondwana Research* 28, 581-600.
- Royer, J.-Y., Chaubey, A.K., Dymant, J., Bhattacharya, G.C., Srinivas, K., Yatheesh, V., Ramprasad, T., 2002. Paleogene plate tectonic evolution of the Arabian and Eastern Somali basins. *Geological Society, London, Special Publications* 195, 7-23.
- Sandwell, D.T., MacKenzie, K.R., 1989. Geoid height versus topography for oceanic plateaus and swells. *Journal of Geophysical Research: Solid Earth* 94, 7403-7418.
- Sandwell, D.T., Müller, R.D., Smith, W.H.F., Garcia, E., Francis, R., 2014. New global marine gravity model from CryoSat-2 and Jason-1 reveals buried tectonic structure. *Science* 346, 65-67.
- Sandwell, D.T., Renkin, M.L., 1988. Compensation of swells and plateaus in the north Pacific: No direct evidence for mantle convection. *Journal of Geophysical Research: Solid Earth* 93, 2775-2783.
- Singh, A.P., 1999. The deep crustal accretion beneath the Laxmi Ridge in the northeastern Arabian Sea: the plume model again. *Journal of Geodynamics* 27, 609-622.
- Sreejith, K.M., Krishna, K.S., 2013. Spatial variations in isostatic compensation mechanisms of the Ninetyeast Ridge and their tectonic significance. *Journal of Geophysical Research: Solid Earth* 118, 5165-5184.

- Sreejith, K.M., Rajesh, S., Majumdar, T.J., Srinivasa Rao, G., Radhakrishna, M., Krishna, K.S., Rajawat, A.S., 2013. High-resolution residual geoid and gravity anomaly data of the northern Indian Ocean – An input to geological understanding. *Journal of Asian Earth Sciences* 62, 616-626.
- Talwani, M., Reif, C., 1998. Laxmi Ridge – A continental sliver in the Arabian Sea. *Marine Geophysical Researches* 20, 259-271.
- Talwani, M., Worzel, J.L., Landisman, M., 1959. Rapid gravity computations for two-dimensional bodies with application to the Mendocino submarine fracture zone. *Journal of Geophysical Research* 64, 49-59.
- Tiwari, V.M., Grevemeyer, I., Singh, B., Phipps Morgan, J., 2007. Variation of effective elastic thickness and melt production along the Deccan–Reunion hotspot track. *Earth and Planetary Science Letters* 264, 9-21.
- Todal, A., Edholm, O., 1998. Continental margin off Western India and Deccan Large Igneous Province. *Marine Geophysical Researches* 20, 273-291.
- Watts, A.B., 1978. An analysis of isostasy in the world's oceans 1. Hawaiian-Emperor Seamount Chain. *Journal of Geophysical Research: Solid Earth* 83, 5989-6004.
- Watts, A.B., 1988. Gravity anomalies, crustal structure and flexure of the lithosphere at the Baltimore Canyon Trough. *Earth and Planetary Science Letters* 89, 221-238.
- Watts, A.B., 2001. *Isostasy and Flexure of the Lithosphere*. Cambridge University Press.
- Won, I.J., Bevis, M., 1987. Computing the gravitational and magnetic anomalies due to a polygon; algorithms and Fortran subroutines. *GEOPHYSICS* 52, 232-238.
- Watts, A.B., Fairhead, J.D., 1997. Gravity anomalies and magmatism along the western continental margin of the British Isles. *Journal of the Geological Society* 154, 523-529.
- Yatheesh, V., Bhattacharya, G.C., Dymant, J., 2009. Early oceanic opening off Western India–Pakistan margin: The Gop Basin revisited. *Earth and Planetary Science Letters* 284, 399-408.
- Yatheesh, V., Bhattacharya, G.C., Mahender, K., 2006. The terrace like feature in the mid-continental slope region off Trivandrum and a plausible model for India–Madagascar juxtaposition in immediate pre-drift scenario. *Gondwana Research* 10, 179-185.

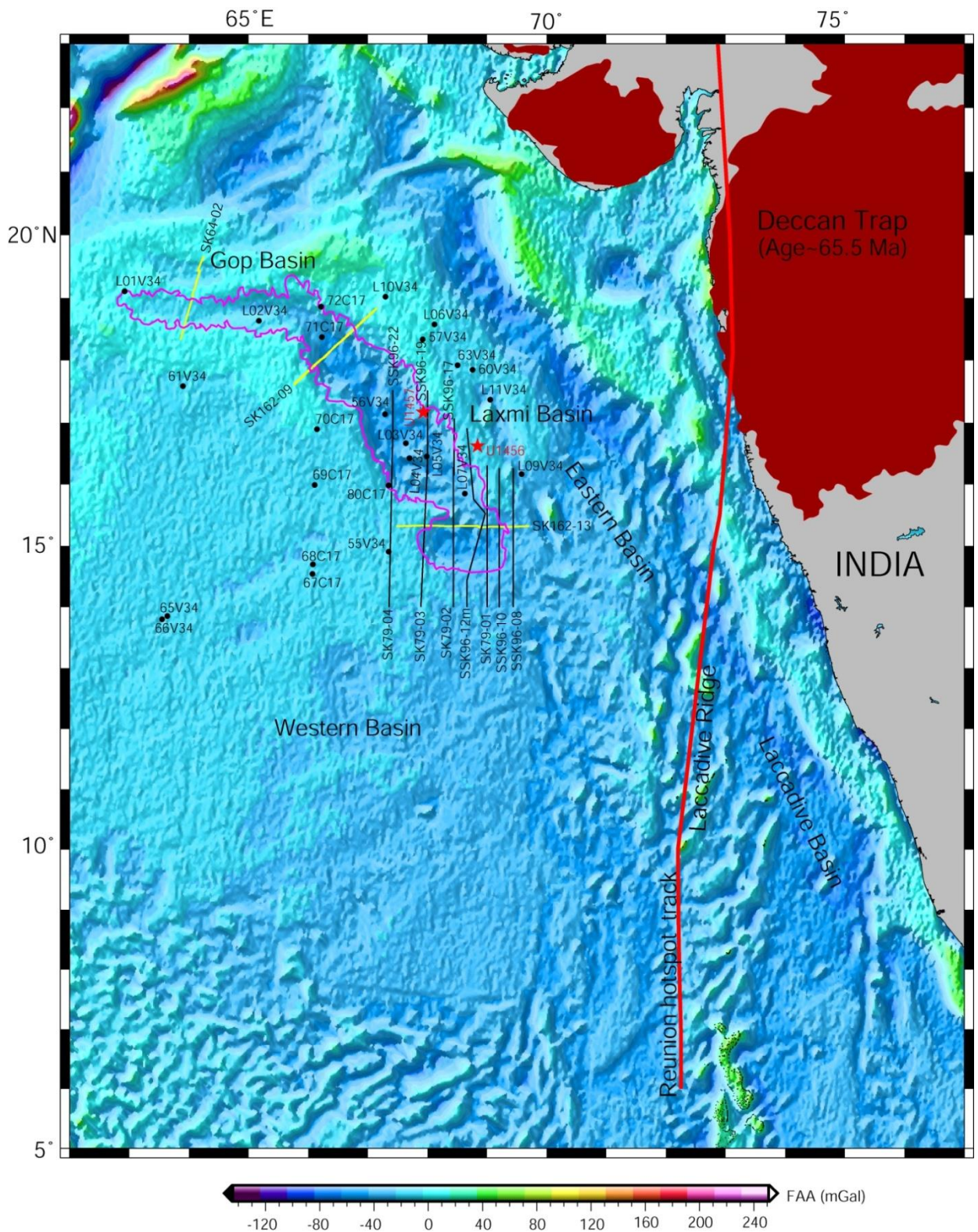


Fig. 1 Satellite-derived free air gravity anomaly map (Sandwell et. al., 2014) of the northern Arabian Sea. Shipborne bathymetry and gravity profiles are shown with yellow lines along which 2D crustal structure has been modeled and shipborne magnetic profiles are shown with black color lines. Red-shaded area represents Deccan Basalt and red line shows Réunion hotspot track. Black circles denote refraction stations compiled from Naini and Talwani (1983). Red stars denote IODP 355 drilling sites. Laxmi Ridge boundary is marked with magenta color line.

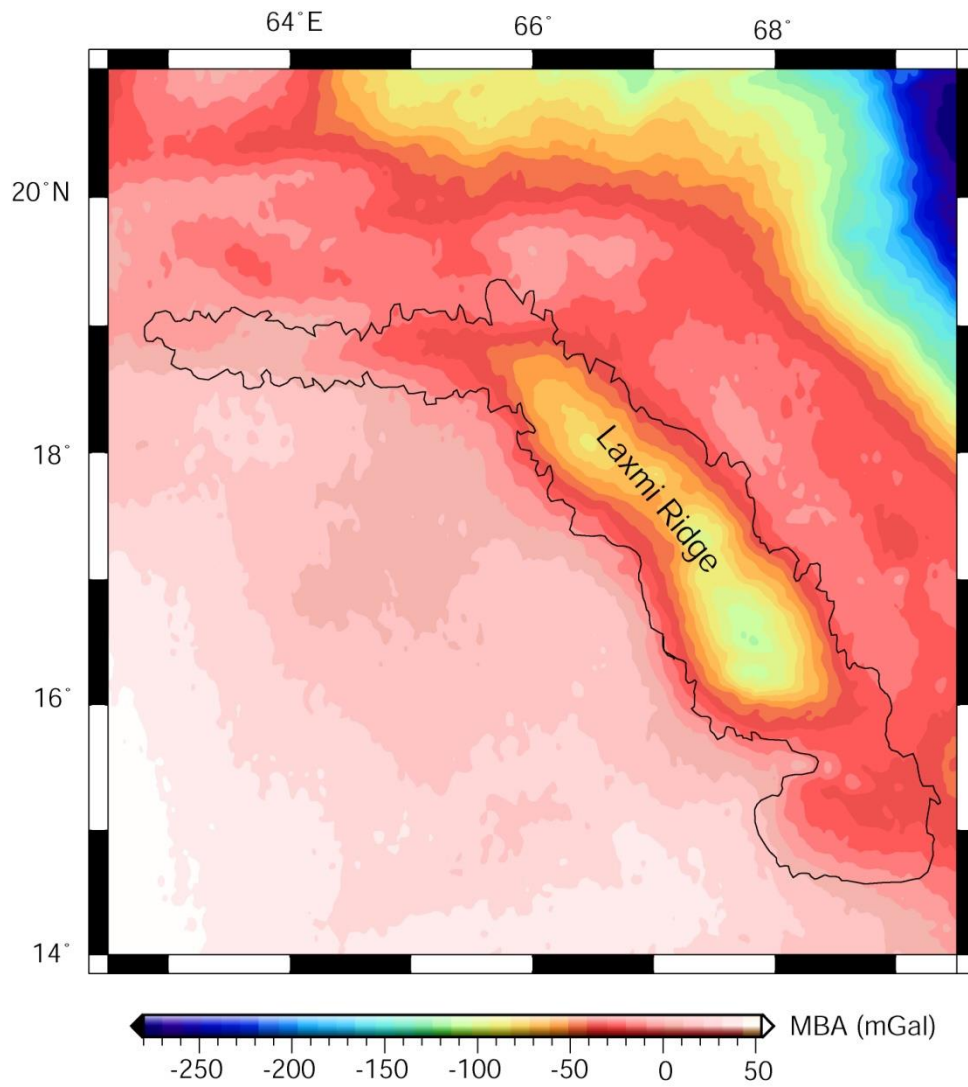


Fig. 2 Mantle Bouguer Anomaly map of the study area. Laxmi Ridge boundary is marked with black line.

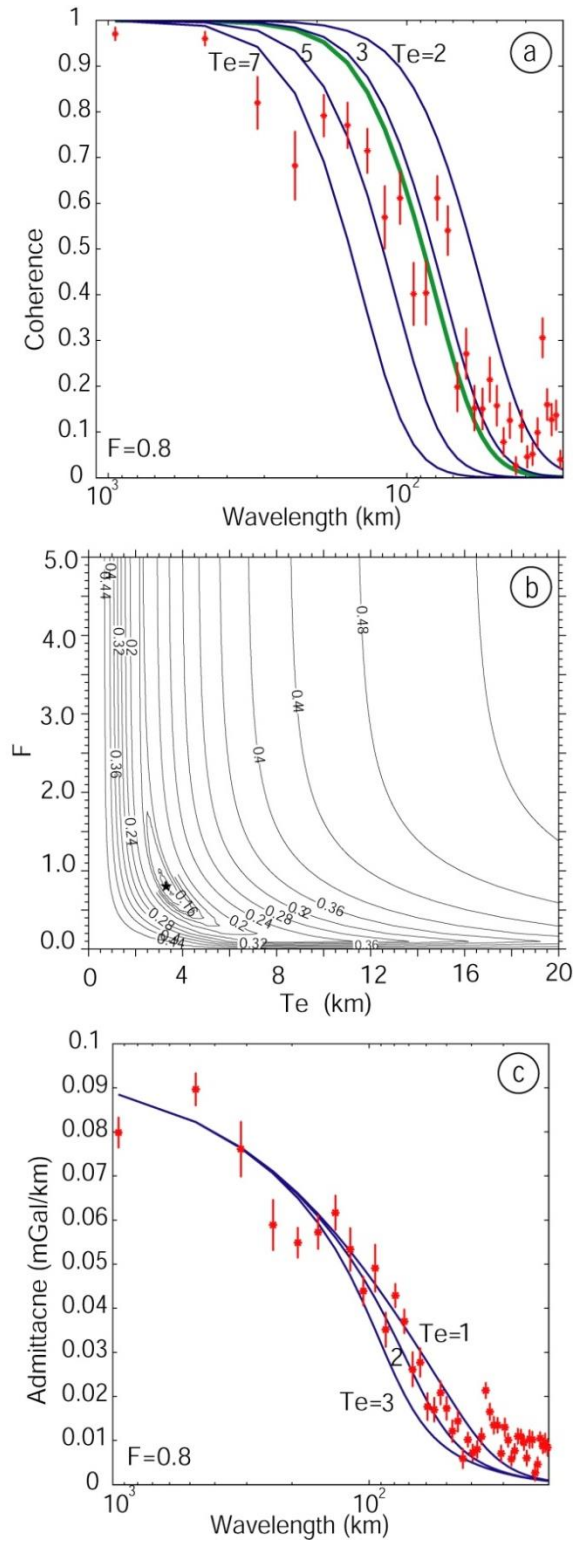


Fig. 3 (a) Plot of observed coherence (red star with error-bar) between MBA and corrected bathymetry, and theoretical coherence curves (blue) for T_e values 2, 3, 5 and 7 km assuming $F=0.8$, (b) RMS plot of the misfit between theoretical and observed coherence as a function of T_e and F . Black star shows minimum value of RMS which corresponds to $T_e=3.3$ km and $F=0.8$, (c) Plot of observed admittance (red star with error-bar) and theoretical admittance curves (blue) for $T_e=1, 2$ and 3 km taking $F=0.8$. The green curve in coherence plot corresponds to the best fit $T_e=3.3$ km and $F=0.8$.

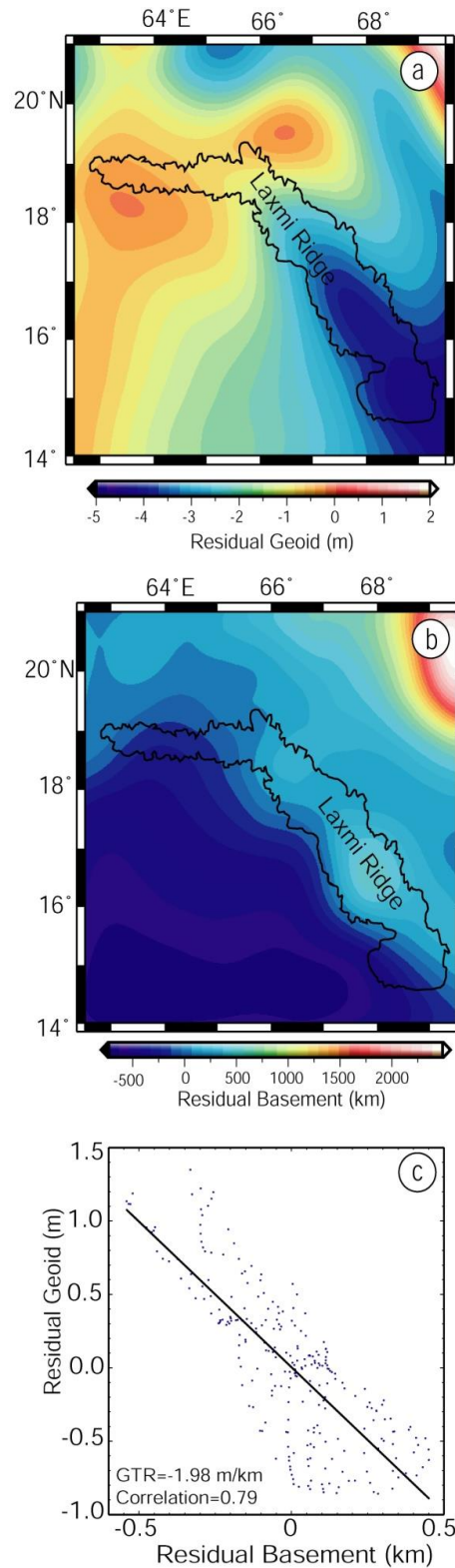


Fig. 4 (a) Residual geoid anomaly calculated by filtering the geoid (EGM2008) in wavelength-band 330-4000 km. (b) Residual basement calculated by filtering corrected bathymetry in wavelength-band 330-4000 km. (c) Scatter plot between residual geoid and residual basement in wavelength-band 330-4000 km; black line is the best fit line which gives geoid to topography ratio (GTR). The Laxmi Ridge boundary in (a) and (b) has been shown with black color curve.

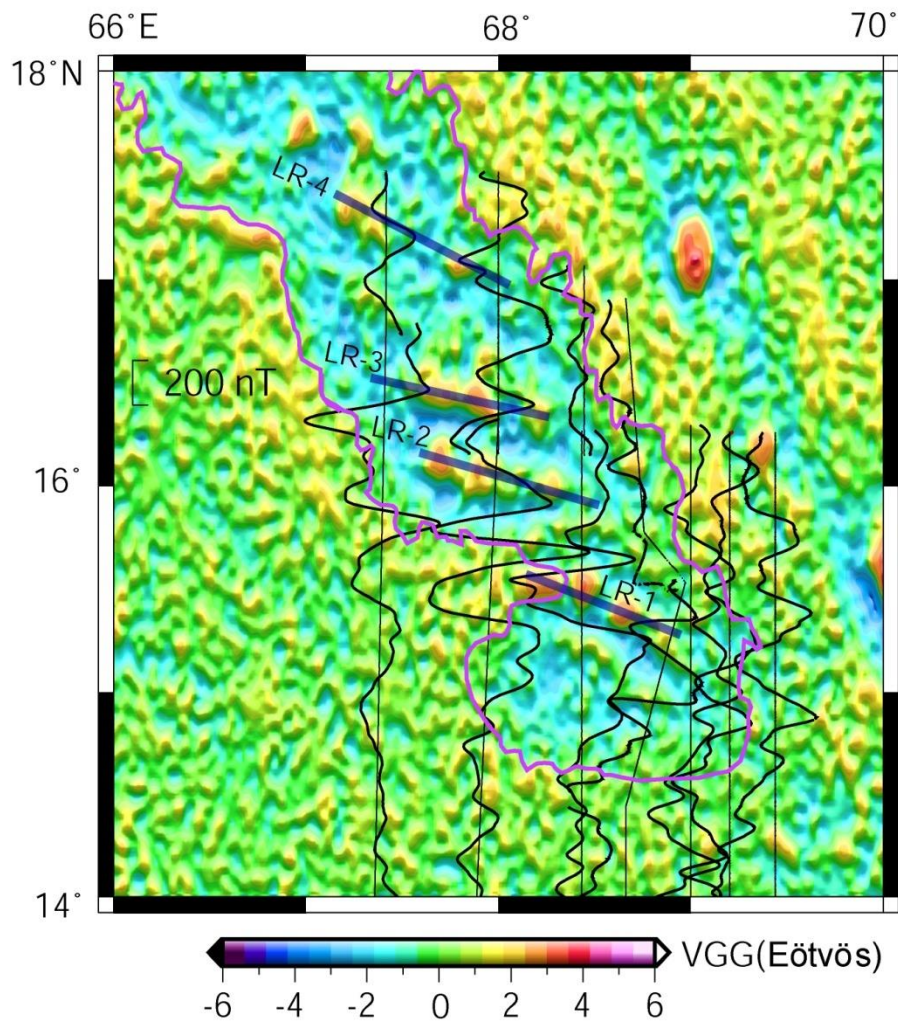


Fig. 5 Magnetic anomaly along several N-S tracks plotted on a histogram equalized vertical gravity gradient map over the southern part of the Laxmi Ridge. LR-1 to LR-4 represent magnetic lineations. Boundary of the Laxmi Ridge is shown with magenta color curve.

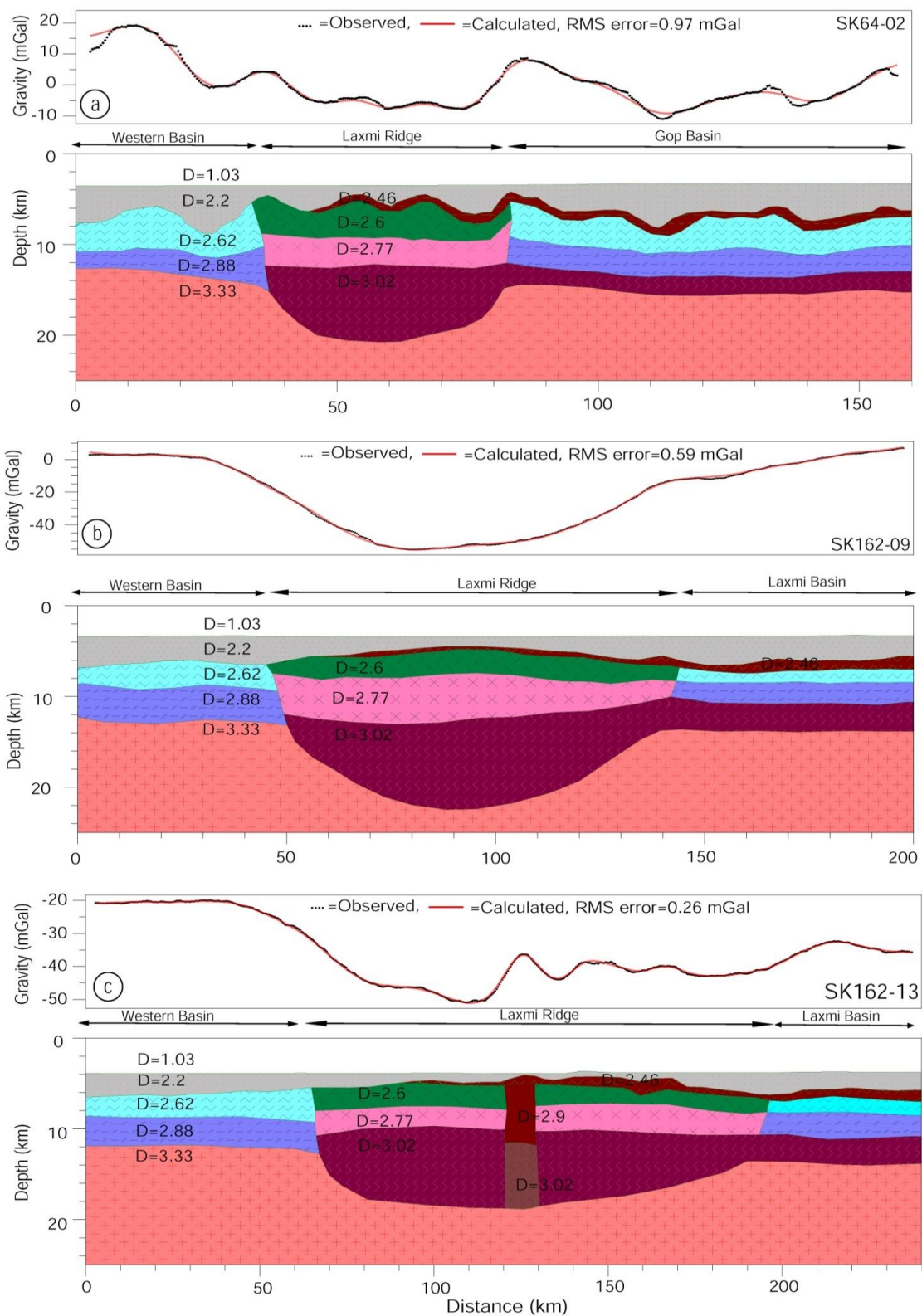


Fig. 6 Crustal models obtained by 2D forward gravity modeling under constraints from published crustal velocity and nearby seismic reflection data. (a) Crustal model along track SK64-02, (b) Crustal model along track SK162-09 and, (c) Crustal model along track SK162-13. D: Crustal density in g/cm^3 .

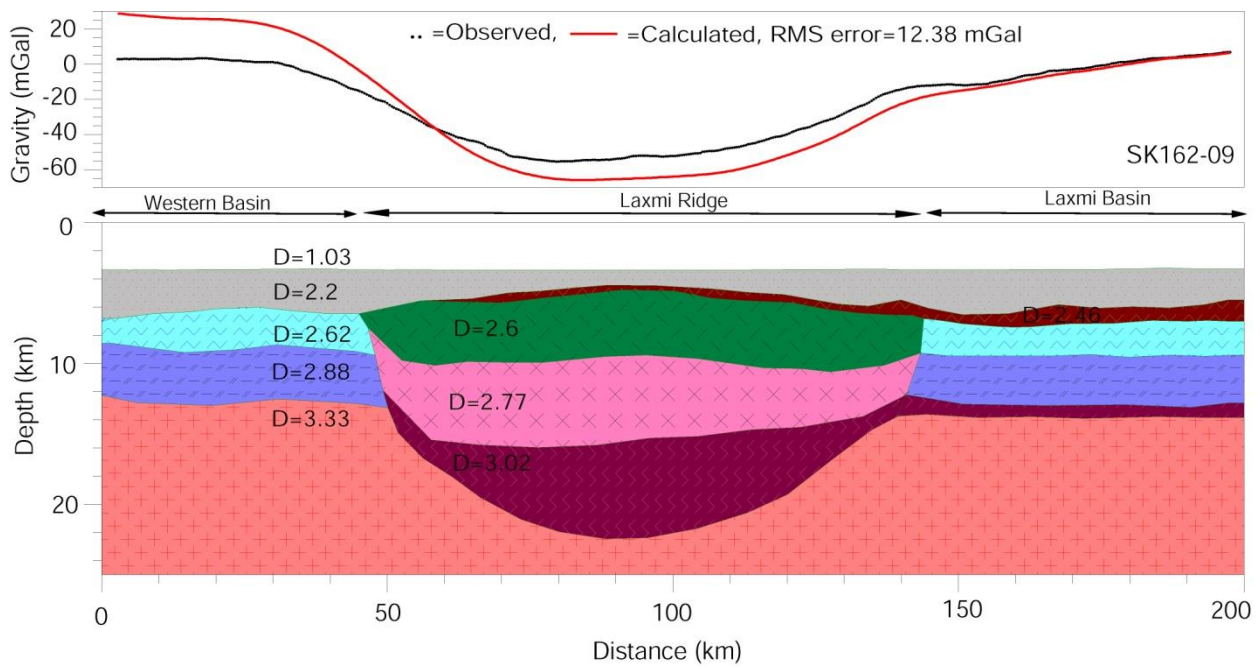


Fig. 7 Uncertainty analysis of 2D forward gravity model along track SK162-09 by reducing 3 km thickness of underplated layer as compared to best fit crustal model (Fig. 6b). It may be noted that a large mismatch occurs between observed and calculated gravity anomalies. RMS error is increased to 12.38 mGal as compared to 0.59 mGal of the best fit model (Fig. 6b).

List of Tables

Table 1 Average P-wave velocity in different crustal layers. Densities for each layer is calculated using Brocher (2005) formula.

Crustal Layers	Average velocity (km/s)	Density (g/cm³)
Flood Basalt	4.50	2.46
Oceanic Layer-2	5.51	2.62
Oceanic Layer-3	6.67	2.88
Crustal Layer-1	5.43	2.60
Crustal Layer-2	6.30	2.78
Underplating	7.20	3.03
Mantle	8.10	3.33

Table 2 Model parameters used for calculation of theoretical coherence and admittance.

Parameter	Notation	Value
Density of sea-water	ρ_w	1.03 g/cm ³
Density of crust	ρ_c	2.70 g/cm ³
Density of mantle	ρ_m	3.30 g/cm ³
Young's modulus	E	100 Gpa
Poisson's ratio	σ	0.25
Universal gravitational constant	G	6.67x10 ⁻¹¹ N m ² kg ⁻²
Acceleration due to gravity	g	9.81 m/s ²
Average Moho depth	d	11 km

Table 3 List of plateaus/ridges with negative GTR.

S. No.	Plateau/ Ridge	GTR (m/Km)	References
1.	Rockall Plateau	-0.173, -1.172	Sandwell and Mackenzie, 1989; Marks and Sandwell, 1991.
2.	Voring Plateau	-0.45, -0.32	Marquart, 1991; Heller and Marquart, 2002.
3.	Shirshov Plateau	-1.008, -2.996	Sandwell and Mackenzie, 1989; Marks and Sandwell, 1991
4.	85° E Ridge (near 14° N)	-1.00	Rao et al., 2016
5.	Laxmi Ridge	-1.98	Present Study